X-RAY TOPOGRAPHY OF LASER ANNEALED ION IMPLANTED SILICON CRYSTALS

by

ARGENIS PRIETO

Lic. en Fisica - Unversidad de Oriente, 1979
Cumana, Venezuela

A MASTER'S THESIS

submitted in partial fulfillment of the

requirements for the degree

MASTER OF SCIENCE

Department of Physics

KANSAS STATE UNIVERSITY

Manhattan, Kansas

1983

Approved by:

Major Professor

THIS BOOK
CONTAINS
NUMEROUS PAGES
WITH THE ORIGINAL
PRINTING BEING
SKEWED
DIFFERENTLY FROM
THE TOP OF THE
PAGE TO THE
BOTTOM.

THIS IS AS RECEIVED
FROM THE
CUSTOMER.

TABLE OF CONTENTS

ACKNOWLEDGEMENTS

I like to thank my wife, Rosemary, for her love and support.

I am also deeply indebted to my major professor, Dr. R. D. Dragsdorf, for his continuous support and enthusiasm during this work.

LIST OF FIGURES

LIST OF PLATES

LIST OF TABLES

Chapter 1

INTRODUCTION

Ion Implantation

In the process of ion implantation an accelerated beam of ions is incident onto a crystal. These ions have been accelerated by a high voltage difference and therefore carry a significant amount of energy when they strike the crystal. During the interaction process, the ions are slowed within the crystalline lattice by displacing a number of atoms and thus altering the geometry of the crystal.

The purpose of ion implantation is the introduction of ions into the crystal lattice for the alteration of various properties (electrical, mechanical, chemical, optical, etc.) of the crystal. Desirable properties of crystals are then obtained by introducing ions (impurities) into the crystal in a controlled way.

We have then two main results of ion implantation, lattice damage and the introduction of desired impurity ions into crystals.

Usually the introduction of impurities in semiconductors is done by diffusion.[1] This is achieved in two steps: deposition and then diffusion. In the first step a layer of the dopant is placed on the crystal surface. Secondly, the crystal is placed in a high temperature furnace, below the melting point of the material involved, in a gaseous atmosphere of oxygen or nitrogen. Diffusion then takes place. It is worth noting that several factors are important and need to be tightly controlled: dopant concentration and thickness, temperature and pressure of the gas, and time.

The ion implantation has the advantage of being easier to control and ions can be embedded at greater depths than those reached by diffusion during a comparable time. However, ion implantation has the disadvantage of producing damage in the crystal, which is usually removed almost totally by annealing.

Silicon, a widely used crystal in semiconductor technology, as a member of Group IV, has four electrons in its outer shell (M). Silicon is usually doped with boron, phosphorous, arsenic and antimony (Group V) as donors and with lithium, aluminum, gallium and indium (Group III) as acceptors; thus obtaining n and p type silicon, respectively.

The range or depth of ions introduced in the implantation process is determined by the ions initial energy and the rate of energy loss in the crystal. Ion range, for different species with various energies have been tabulated[2] for different crystals using the Lindhard, Scharff and Schiott method.[3]

The region of lattice damage roughly is that through which the ions have passed while being slowed down by collisions with the lattice atoms.

Annealing

As ions penetrate the crystal lattice in the ion implantation process they lose energy in their interactions with the atoms of the crystal until they come to rest inside of it. A typical valve of the energy required to displace an atom from its position in the lattice is on the order of $\sim$25 eV. Ions with energies of the order of KeV can therefore cause an extensive damage to the lattice, displacing a large number of the base material ions.

The process by which the geometry of the crystal is restored is called annealing. In the ideal crystal structure the atoms are arranged at their minimum energy configuration. By absorbing energy from the incident ions the crystal takes on a strained, higher energy, configuration.

To anneal a damaged lattice, energy is introduced to allow the atoms to migrate by surpassing the local binding energy.

Dissipation of strain energy then takes place and the material reforms to its minimum energy configuration.

Two methods are widely used:

i) Oven Annealing. The damaged crystal is heated in an oven and its temperature raised to near the melting point. By absorbing thermal energy, atoms can migrate alleviating the strained configuration characteristic of the damaged crystal. The sample is then allowed to cool and by using an impurity or a substrate as a seed recrystallization takes place.

This is the method normally used in the technology of semiconductors. Good results are obtained with this technique, however there is the inconvenience of having to wait for the crystallization and cooling off of the sample. Another drawback is the fact that after the preparation of an electronic component; the whole component, crystal plus connecting leads, needs to be put into an oven to process the crystal which is not always desirable.

ii) Laser Annealing. In this process a laser beam is used to heat the damaged crystal, thereby inducing the annealing process.

Laser annealing is done on spots of rather small dimensions, diameters of approximately 250 μm[4] are used. The irradiated energy is absorbed and recrystallization of a large fraction of material onto which the laser is incident occurs in $\approx$ 28 n sec in silicon.[4] A great number of overlapping spots are subsequently annealed to process a whole crystal surface.

During this process evidence has been found[5] that the molten crystal picture of annealing might be inappropriate since measurement of the temperature of the annealed spot by the Stokes/anti-Stokes line ratio in Raman scattering spectroscopy gives a value substantially less than that of the melting point.

An advantage of laser annealing is that it can be done on selected small

areas without disturbing neighboring surfaces. Another advantage is the speed with which the process can be carried out and the lower overall energy consumption required.

X-Ray Topography

i) Bragg Geometry. When an incident x-ray beam reaches a perfect crystal, there is a diffracted beam that leaves the crystal from the same face that is struck by the incident beam. Another beam is transmitted through the crystal leaving from the opposite face.

The diffracted beam arises from scattered radiation from atoms that, because of their periodic arrangement, form diffracting planes. In Fig. 1 nearly monochromatic x-rays of wavelenth λ reach the crystal with an angle θ. Ray 1 and Ray 2 will lead to constructive interference if their path difference 1 - 2 is an integer multiple of λ. (d is known as the interplanar spacing.)

From the geometry of Fig. 1, the Bragg's Law $n\lambda=2d \sin \theta$ (1) is obtained.

The planes of a crystal are defined by the Miller indices (h, k, ℓ) and the parameters (a_1, a_2, a_3, α_{12}, α_{23}, α_{31}) associated with the unit cell. In the cubic system,[6] $a_1 = a_2 = a_3 = a$ and $\alpha_{12} = \alpha_{23} = \alpha_{31} = 90^o$, the interplanar spacing is related to the Miller indices by the relation

$$\frac{1}{d^2} = \frac{(h^2 + k^2 + \ell^2)}{a^2} \quad (2)$$

This relationship, along with Bragg's Law, defines the angle θ at which diffraction takes place (Bragg's angle) for the various symmetry planes defined by their Miller indices. From eqs. 1 and 2 the following relationship is obtained:

$$\sin^2\theta = \frac{\lambda^2}{4a^2} (h^2 + k^2 + \ell^2)$$

In x-ray diffraction topography, an x-ray beam incident on a crystal at

THIS BOOK CONTAINS NUMEROUS PAGES THAT WERE BOUND WITHOUT PAGE NUMBERS.

THIS IS AS RECEIVED FROM CUSTOMER.

Figure 1

Path of Ray 1 = $\overline{AB} = \frac{2d}{\sin_B}$

Path of Ray 2 = $\overline{CB} = \frac{2d \cos^2\theta_B}{\sin\theta_B}$

For constructive interference:

$n\lambda = \overline{AB} - \overline{CB} = 2d \sin\theta_B$

THIS BOOK CONTAINS NUMEROUS PAGES WITH DIAGRAMS THAT ARE CROOKED COMPARED TO THE REST OF THE INFORMATION ON THE PAGE.

THIS IS AS RECEIVED FROM CUSTOMER.

FIGURE 1

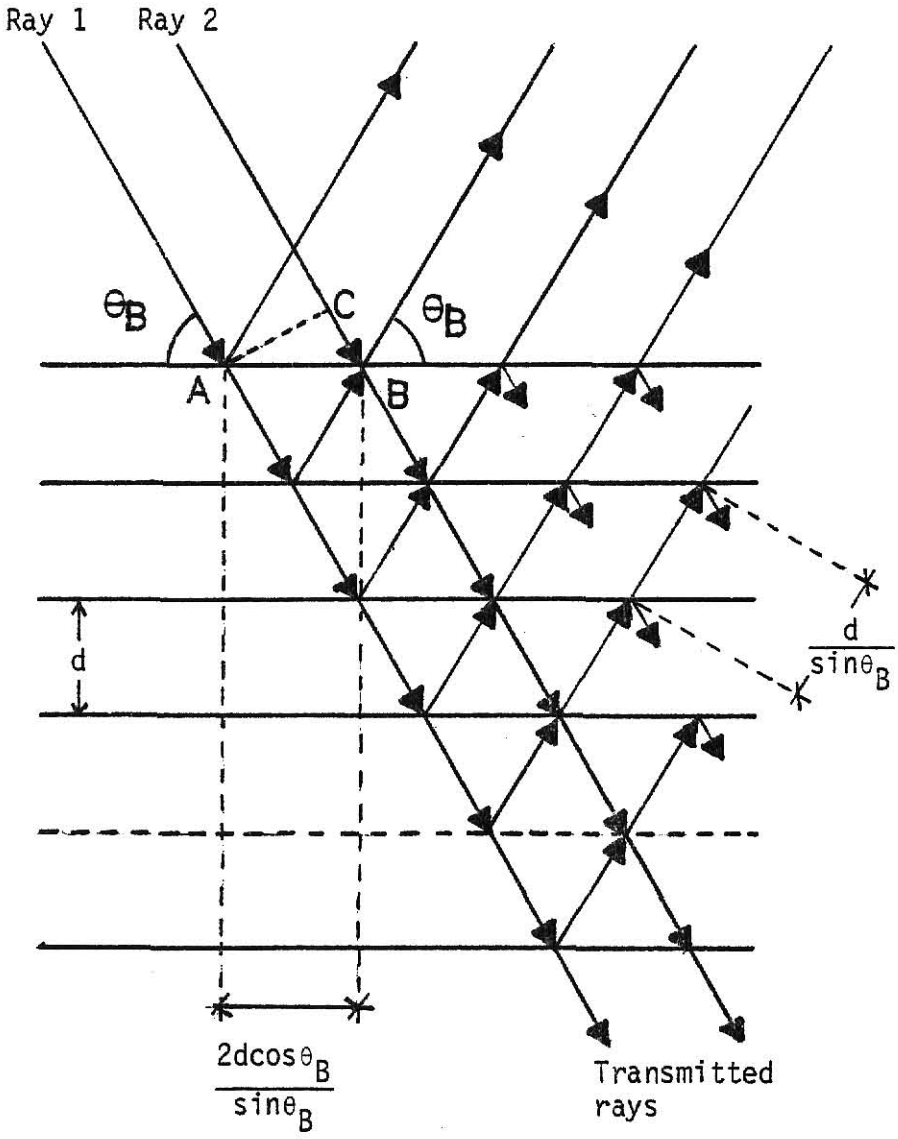
Ray 1
Ray 2
θ_B
C
θ_B
A
B
d
$\frac{d}{\sin\theta_B}$
$\frac{2d\cos\theta_B}{\sin\theta_B}$
Transmitted rays

the Bragg angle (associated with a set of planes) is diffracted and its direction is intercepted by an x-ray film. This is arranged in such a manner that a one-to-one relationship is established between the spot on the crystal and its image on the film. When imperfections are present in the crystal, their corresponding areas on the film show a variation in contrast to those of unstrained or perfect crystal zones. This arises from the variation of the Bragg angle.

An image of the imperfections is thus projected onto the film. The study of the crystal using the diffracted intensity off the surface of the crystal is known as Bragg's Geometry.

ii) Laue Geometry. In this case the beam diffracted by planes leaves the crystal from the opposite face as the transmitted beam. Two cases are distinguished:

a) Case of a Thin Crystal (Fig. 2). The incident x-ray beam is diffracted by a set of planes and after passing through the crystal it is recorded on film. Absorption takes place. For a thin crystal (μ t << 1), μ being the linear absorption coefficient and t the distance traveled by the beam inside of the crystal, the absorption ($\sim 1-e^{-\mu t}$) is not very strong, therefore, the diffracted beam is easily recorded on x-ray film.

Strained zones will give rise to contrast in corresponding areas of the film as there is a variation of the Bragg angle which leads to a variation of the intensity of the diffracted beam.

b) Case of Thick Crystals. Borrmann[6] found that in fairly thick, nearly perfect crystals ($\mu t \simeq 10$) reflection of nearly monochromatic x-ray radiation takes place and the transmitted and diffracted beams have a surprisingly high intensity. This occurs if the incident beam reaches the diffracting planes at exactly the Bragg angle.

Figure 2 Laue Geometry. Thin crystal case.

FIGURE 2

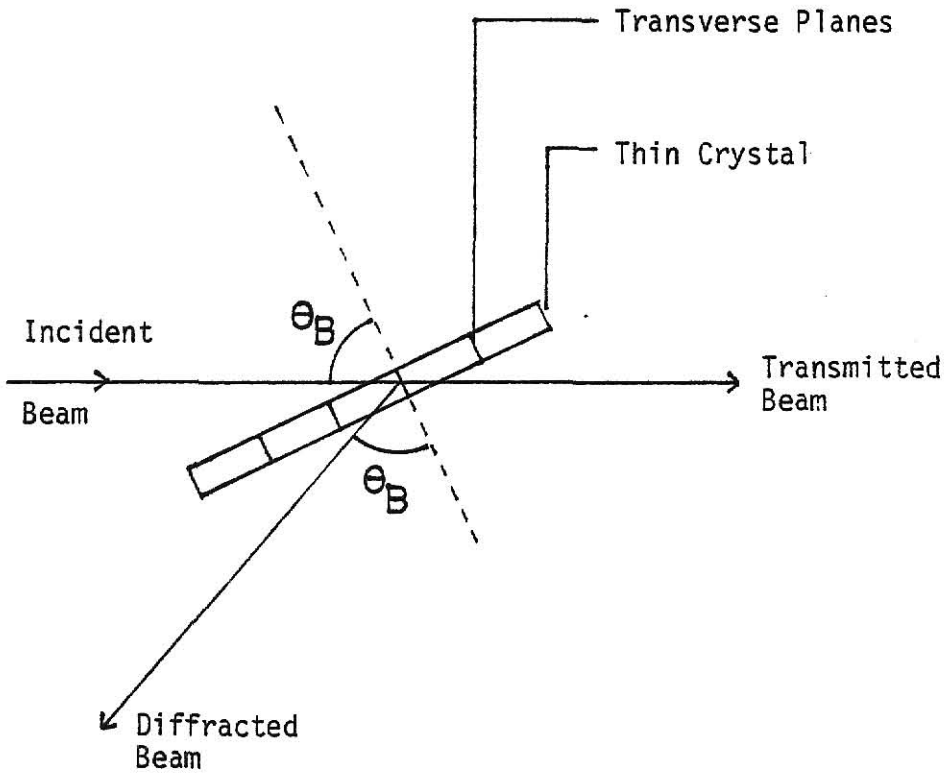
Transverse Planes
Thin Crystal
Incident
Beam
θ_B
Transmitted
Beam
θ_B
Diffracted
Beam

The effect is known as anomalous transmission (Fig. 3).

In this method, both the transmitted and diffracted beam are used to study the structure of the crystal.

Purpose of the Experiment

The objective of this experiment is the study of laser annealed, ion implanted silicon crystals by x-ray topography. These crystals were ion implanted and laser annealed in the Physics Department at Kansas State University.

During the process of laser annealing, done at a number of different spots with different energy/unit area, the Raman spectra yielded temperatures[5] well below that of the melting point of silicon. From other experiments there arose a controversy about the established model of thermal annealing. A. Aydinli et al.[7] of KSU proposed the existence of a self contained plasma in silicon during laser annealing.

Through an experimental set-up, x-ray topographs are obtained and the residual strain of the annealed spots is compared to that of a "perfect" silicon crystal, thus establishing the degree of anneal obtained for the various [energy/unit area] values used. Since laser annealing is done on a very small area it is important to define the annealing surrounding this small area.

This can be accomplished by relating contrast in the micrographs to the strain of the lattice.

Figure 3 Anomalous transmission in thick crystals.

FIGURE 3

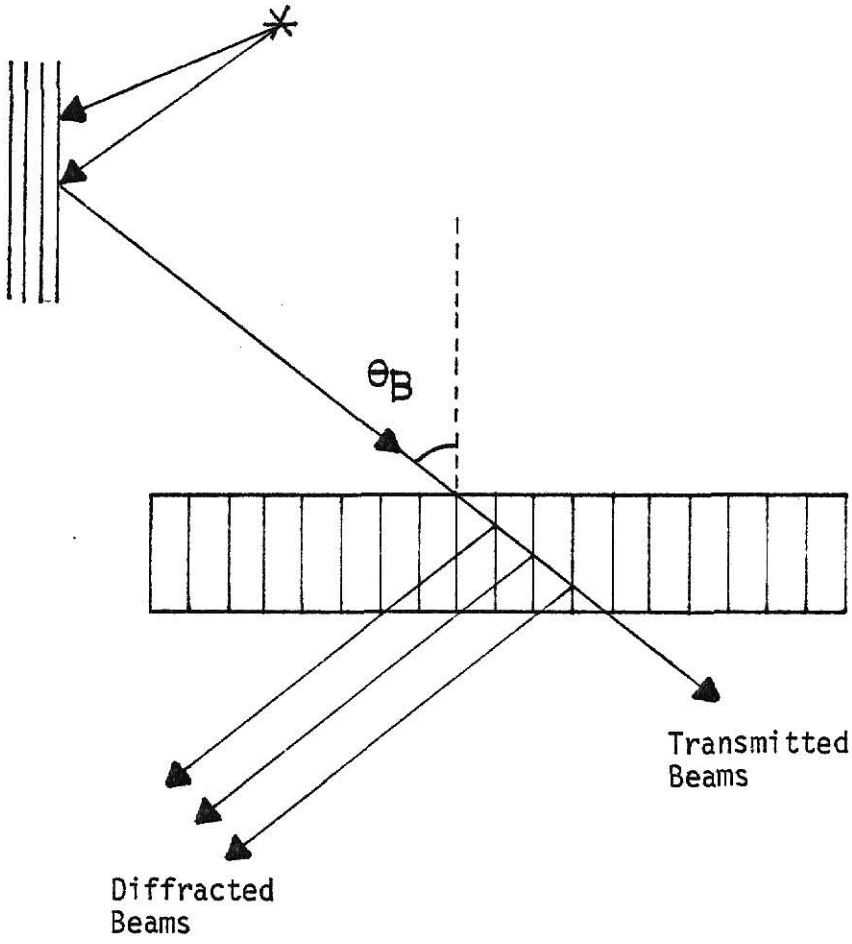

Chapter 2

EXPERIMENT

The Silicon Crystal

Silicon (Z=14) crystallizes in the diamond cubic arrangement.[8] It has an axial length of a=5.43085Å at 20°C.[9] There are 8 atoms per unit cell in the positions 0,0,0; 0,½,½; ½,0,½; ½,½,0; 1/4, 3/4, 3/4; 3/4, 1/4, 3/4; 3/4, 3/4, 1/4; 1/4, 1/4, 1/4. The unit cell of this structure is illustrated in Fig. 4.

The intensity of the diffracted beams, when monochromatic x-rays are incident on the symmetry planes at the respective Bragg angle, depends on the structure factor (F) multiplied by its complex conjugate.

Intensity of diffracted beam $\sim F \cdot F^*$.

$$F = f \sum_n e^{2\pi i(hx_n + ky_n + \ell z_n)}$$

where h, k, ℓ are the Miller indices representing a particular set of planes of symmetry of the crystal. x_n, y_n, z_n represent the position of the atoms in the unit cell.

f is the atomic scattering factor of the particular atom. Information about the intensity of the diffracted beam is then obtained from the calculation of the structure factor.

In Si the structure factor is given by:

$$F = f_{Si}\,[1+e^{\pi i(k+\ell)}+e^{\pi i(h+\ell)}+e^{\pi i(h+k)}+e^{\frac{\pi i}{2}(h+k+\ell)} + e^{\frac{\pi i}{2}(h+3k+3\ell)}+e^{\frac{\pi i}{2}(3h+k+3\ell)}+e^{\frac{\pi i}{2}(3h+3k+\ell)}]$$

$$= f_{Si}\,[(1+e^{\pi i(k+\ell)}+e^{\pi i(h+\ell)}+e^{\pi i(h+k)})\,(1+e^{\frac{\pi i}{2}(h+k+\ell)})]$$

Case I: Mixed Indices (even and odd numbers in h, k, ℓ).

Figure 4 The diamond type silicon unit cell.

FIGURE 4

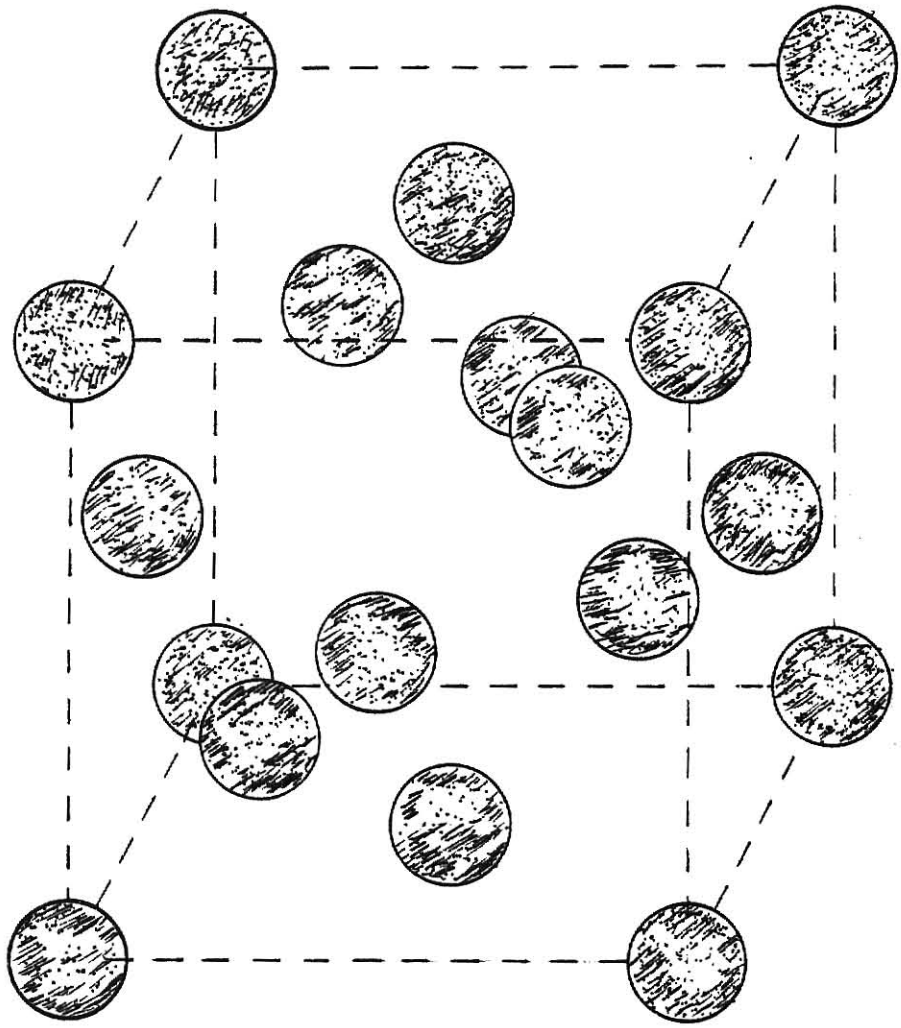

$$1+(e^{\pi i(k+\ell)}+e^{\pi i(h+\ell)}+e^{\pi i(h+k)}) = 0$$

Then, F=0 and FF*=0 → there is no diffracted intensity from planes with mixed Miller Indices.

Case II: Unmixed Indices (all even or all odd). In this case, h+k, h+ℓ, k+ℓ are even numbers, therefore

$$1+e^{\pi i(h+k)}+e^{\pi i(h+\ell)}+e^{\pi i(k+\ell)} = 4$$

a) If h+k+ℓ=2n (even) and n is even: $e^{\frac{\pi i}{2}(h+k+\ell)} = 1$

$F=8f_{Si}$; $FF^*=64f_{Si}^2$

If n=odd then

$1+e^{\frac{\pi i}{2}(h+k+\ell)} = 1-1=0$

F=0, FF*=0; therefore there is no diffracted intensity from planes with unmixed indices with a sum that is an even multiple of an odd number.

b) If h+k+ℓ=2n+1 (odd)

$1+e^{\frac{\pi i}{2}(h+k+\ell)}=1+e^{n\pi i}e^{\frac{\pi i}{2}}$

If n is even: $e^{n\pi i}=1$, $F=4f_{Si}(1+i)$

If n is odd: $e^{n\pi i}=1$, $F=4f_{Si}(1-i)$

For n even or odd $FF^* = 16f_{Si}^2\ (2)=32f_{Si}^2$.

Then we can expect reflection from planes whose Miller indices are all even or all odd and, (i) their sum is an even multiple of an even number, or (ii) their sum is odd.

Since Si is a cubic crystal the Bragg angle for diffracting planes with Miller indices h,k,ℓ is given by

$$\sin^2\theta_B = \frac{\lambda^2}{4(5.43085)^2}\ (h^2+k^2+\ell^2)$$

λ: wavelength of the monochromatic incident x-ray radiation ([λ]=Å=10^{-8}cm).

and the interplanar spacing (d) is given by:

$$\frac{1}{d^2} = \frac{(h^2+k^2+\ell^2)}{(5.43085)^2} \qquad [d]=\text{Å}=10^{-8}\text{cm}$$

Crystals used in these Experiments

Specimen A is a single silicon crystal (100) on sapphire, 1.1μ thick, doped with n type phosphorous (5×10^{13} cm^{-3}), and Si^+ implanted at 180 KeV with a dosage of 1×10^{15} ions/cm^2.

The first set of parallel planes to (100) yielding a non-zero structure factor are represented by the Miller indices (400).

$$F_{400}=8f_{Si} \rightarrow F_{400}^2=64f_{Si}^2$$

From Johnson's tables, using the LSS method, the projected range of the implanted ions is $R_p=0.246\mu$ with a nuclear energy loss of 2.45×10^2 KeV/μ, and electronic loss of 3.73×10^2 KeV/μ. The total energy loss as calculated from the projected range is 1.52×10^2 KeV.

This crystal was laser annealed on different spots with different amounts of energy densities varying from 0.08 J/cm^2 to 1.24 J/cm^2. A sketch of the crystal with the labeling of these spots is given in Fig. 5, while the values of the respective energy densities are given in Table I.

With the given dosage of 1.0×10^{15} ions/cm^2 and a projected depth of 0.246μ, a density of 4.0×10^{19} ions/cm^3 is obtained.

Specimen B is a single silicon (100) crystal, As^+ ion implanted at 200 KeV with a dosage of 1×10^{15} ions/cm^2. This crystal was laser annealed on neighboring spots that define a broad area on the crystal surface, and it was also laser annealed at various other spots with different energy densities. In Fig. 6 a sketch of the surface of this crystal is presented, while the labeled spot's annealing energy densities are shown in Table II.

Figure 5 Sketch of Specimen A. Labeling of annealed spots.

FIGURE 5

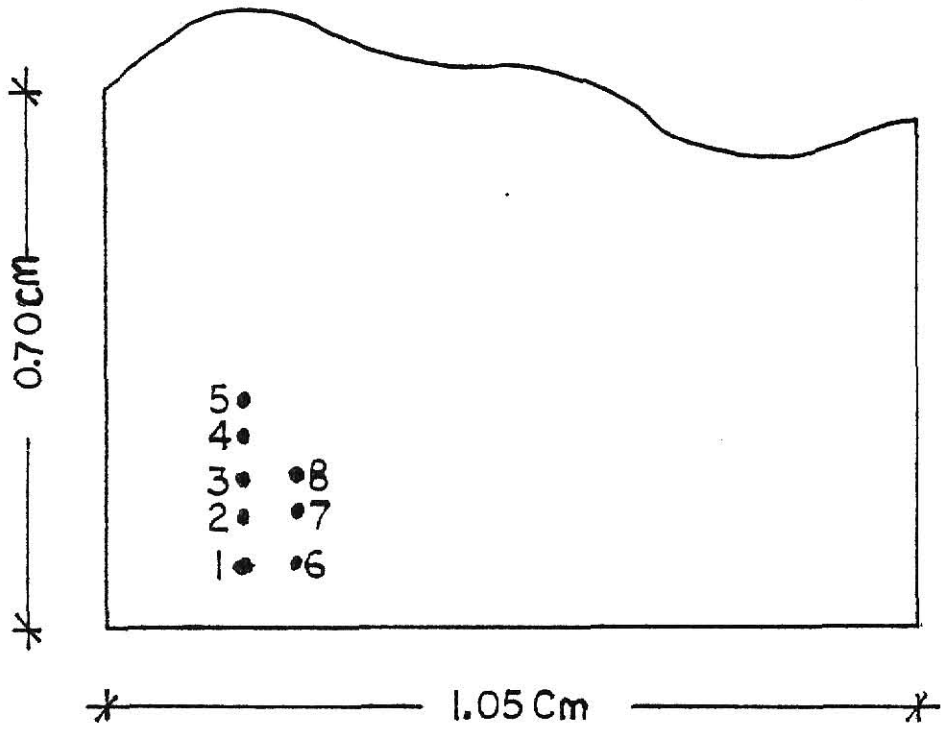

Table 1 Laser energy densities corresponding to labeled spots. Specimen A

TABLE 1

Laser Energy Densities Corresponding to Labeled Spots. Specimen A

Spot #	Energy Density of Laser (J/cm^2)
1	Not available
2	1.15
3	0.81
4	0.57
5	0.39
6	0.21
7	0.08
8	0.21

Figure 6 Sketch of Specimen B. Labeling of annealed spots.

FIGURE 6

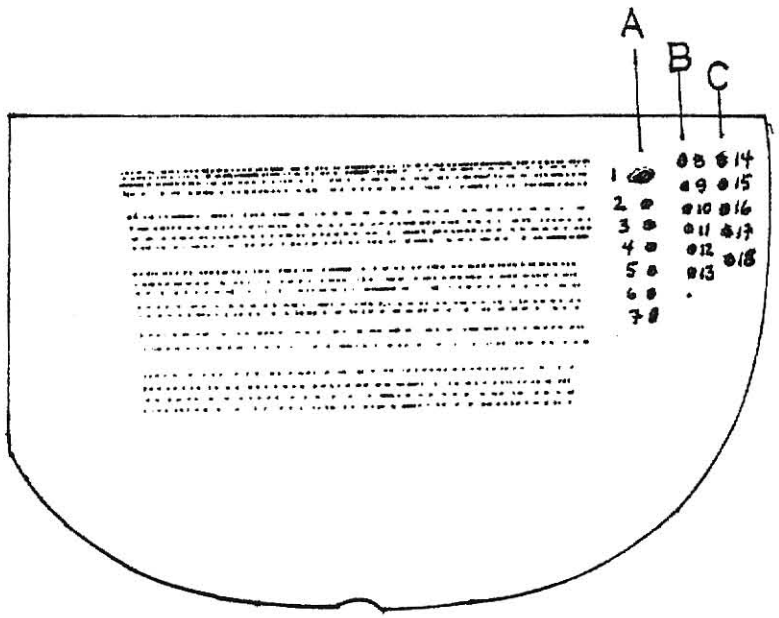

Table 2 Laser energy densities corresponding to labeled spots. Specimen B.

TABLE 2

Laser Energy Densities Corresponding to Labeled Spots. Specimen B

	Spot #	Energy Density of Laser J/cm^2
A	1	4.6
	2	2.3
	3	1.7
	4	1.2 (2 shots, 1.2 each)
	5	1.2
	6	0.69
	7	0.22 (2 shots, 0.22 each)
B	8	1.7
	9	0.9
	10	0.7
	11	0.5
	12	0.3
	13	0.1
C	14	1.7
	15	0.9
	16	0.7
	17	0.5
	18	0.3

From the Johnson's Tables, the projected range of the implanted ions is R_p=0.11μ, with nuclear energy loss of 1285 KeV/μ and an electronic energy loss of 400 KeV/μ. This yields a total energy loss of 185.35 KeV.

As in the case of specimen A, the structure factor $F_{400}=8f_{Si}$, $F^2_{400} = 64f^2_{Si}$.

With a dosage of 1.0×10^{15} ions/cm^2 and a projected range of 0.11μ, the ion density of the implanted profile is 9.09×10^{19} ions/cm^3. Since the atomic density of silicon is 5×10^{22} atoms/cm^3, the ion densities in both cases are obviously important. The ion implantation has the effect of increasing the interplanar spacing of the crystal.

In pure silicon (cubic system)

$$\frac{1}{d^2}=\frac{h^2+k^2+\ell^2}{a^2} \qquad d_{400}=1.35771\text{Å}$$

Geometry of the Experiment

The x-ray source is copper Kα radiation (Ni filtered) which is collimated by a two slit system. The radiation reaches the crystal at the Bragg angle and the diffracted beam is recorded on film. The crystal and the film surfaces are placed parallel to each other on a platform that moves along a horizontal line, back and forth, such that this direction is parallel to the crystal surface. Figures 7 and 8 give a top and side view of the system, respectively.

The horizontal divergence due to the width of the slits A and B, 0.144mm and 0.214mm, respectively, and the length of the collimator was calculated to be 7.15 minutes of arc. The vertical divergence due to the height of slits A and B, 1.1 cm and 2.2 cm, respectively, and the length of the collimator was calculated to be 3.77 degrees of arc.

For the planes represented by Miller indices (400) the corresponding

Figure 7 Geometry of the experiment. Top View.

FIGURE 7

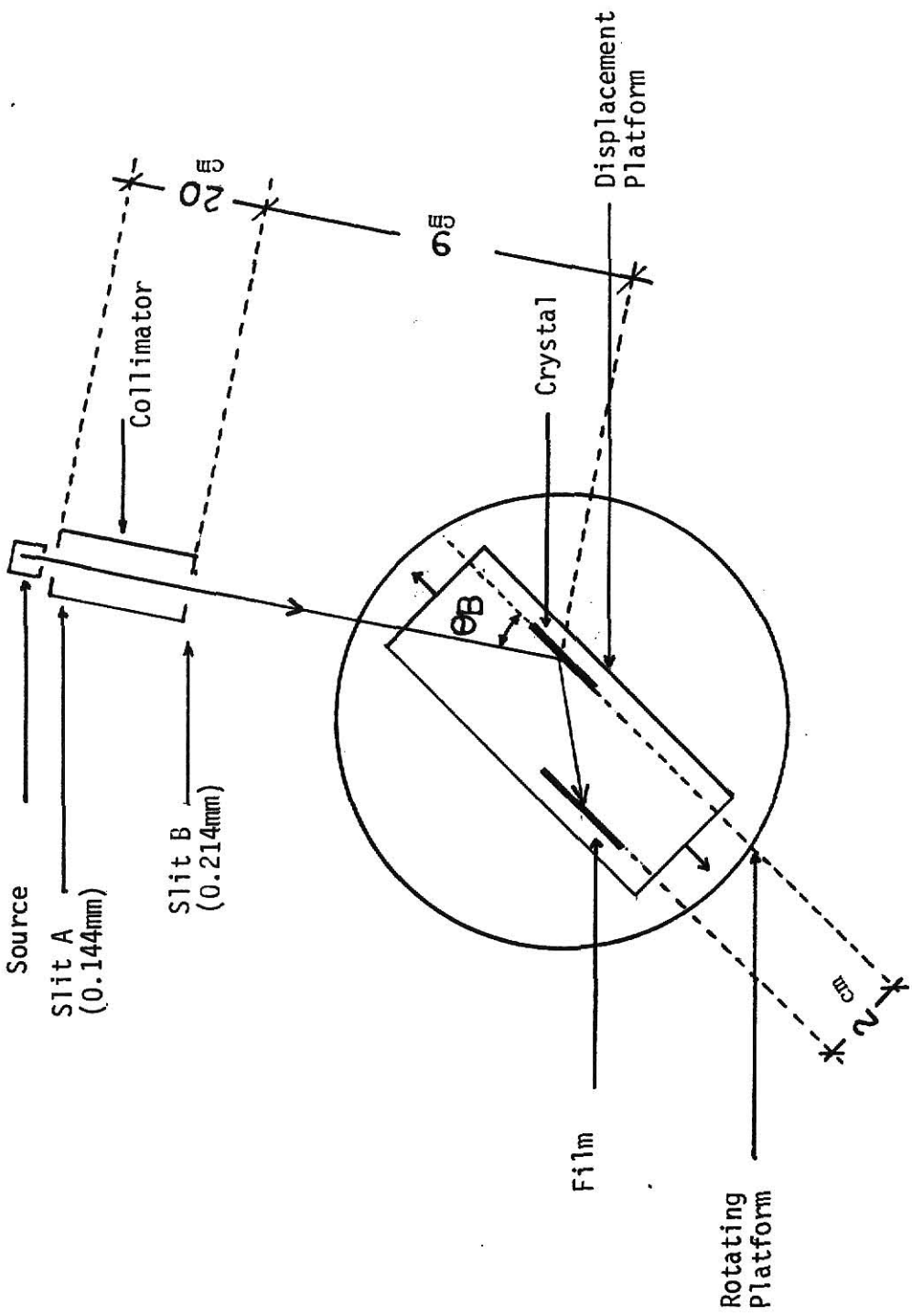
Source
Slit A
(0.144mm)
Slit B
(0.214mm)
Collimator
2θ
θB
Crystal
Displacement
Platform
Film
Rotating
Platform

Figure 8 Geometry of the experiment. Side view.

FIGURE 8

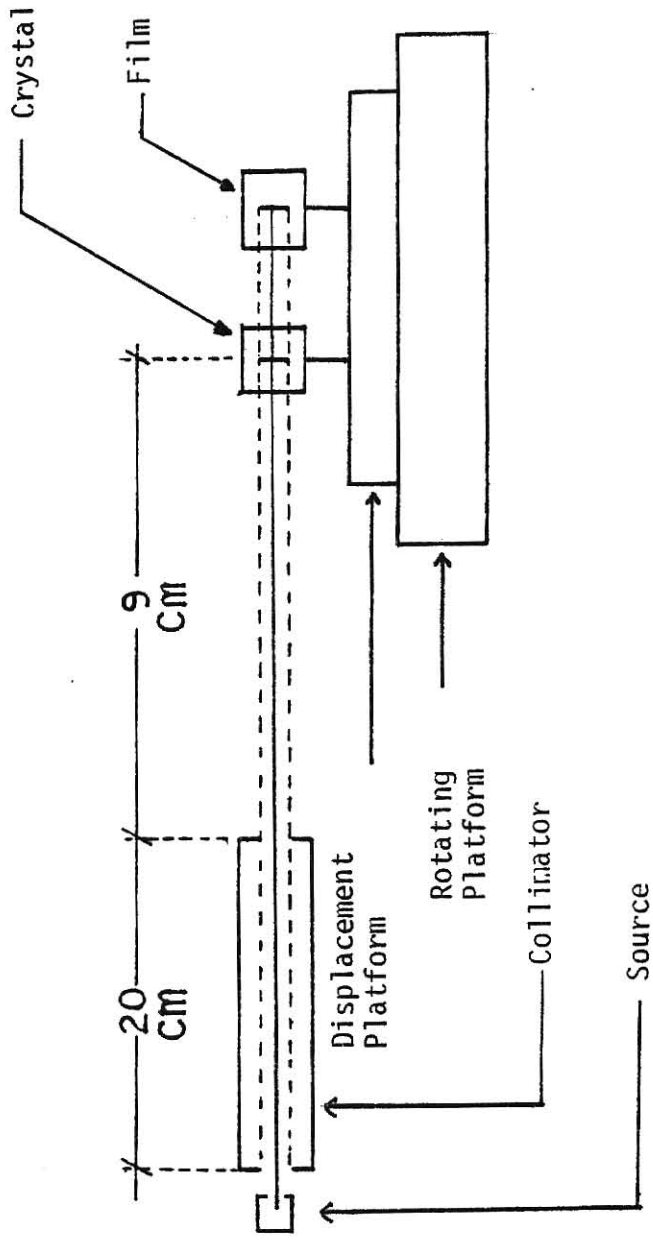
Crystal
Film
9 Cm
20 Cm
Displacement Platform
Rotating Platform
Collimator
Source

Bragg angle is obtained from the relation

$$\sin^2\theta_B = \frac{\lambda_{k\alpha}^2}{4a^2}(h^2+k^2+\ell^2)$$

$$\lambda_{k\alpha} = \frac{2\lambda_{k\alpha 1} + \lambda_{k\alpha 2}}{3} = 1.541838\text{Å} \text{ (weighted average of } \lambda_{k\alpha 1} \text{ and } \lambda_{k\alpha 2})$$

Then,

θ_B = 34.59746 degrees of arc.

Orientation of the Crystal

The crystal is placed on a tilting support that allows adjustments for verticality. This tilting support rests on a displacement platform which also supports the film. Therefore, when the displacement platform moves back and forth, the photographic film and the crystal remain at rest with respect to each other.

Initially the system is placed so that the plane formed by the slits A and B contains the plane of the surface of the crystal, this is set at zero on the rotating platform. The rotating platform is then turned to the calculated Bragg angle, θ_B = 34.59746 degrees of arc.

The next step consists of aligning a Geiger tube in the approximate direction of the diffracted beam. The source, copper target (35 kV, 18mA), is turned on after taking the necessary safety precautions; lead shield was used to intercept the unwanted scattered and transmitted radiation.

A reading of the counter is then obtained. The Geiger counter is realigned for peak detection. Then the crystal is rocked, or rotated, very slowly to obtain a maximum reading on the Geiger counter. The Geiger counter is once again realigned and a fine tuning is carried out by optimizing the angular position of the crystal. Further optimization of the alignment of the crystal is obtained by varying the

tilt of the crystal so that the highest value of diffracted intensity is recorded by the Geiger counter.

When a rough position of the crystal was obtained, the diffracted beam intensity was too high for the Geiger counter to yield a precise reading since it was off scale. This problem was avoided by placing thin aluminum sheets in front of the slit B to act as absorber and thus take the intensity of this beam to a reading about half the Geiger counter scale. The tube current and voltage were also lowered for this purpose. Once this had been done, an optimization of the angular and tilt position was obtained by very small variations of these variables. The tube current and voltage were increased back to their previous operating values for taking the topographs.

Topographs

Once the crystal is oriented for maximum diffracted intensity at the Bragg angle, this angle of incidence is diminished so that the detected intensity is half of the maximum reading. This is done to obtain a better contrast in the topograph.

A piece of fresh x-ray film is placed in an envelope made of black thick paper to prevent exposure from light. It is then placed (x-ray source off) parallel to the crystal face in a position that allows it to intercept the diffracted beam.

Once the film is in place, the motor that drives the displacement platform and the x-rays are turned on. As the radiating slit scans the surface of the crystal, the corresponding diffracted radiation is absorbed (partially) by the film. Since the blackening of x-ray film is the consequence of intensity (energy) absorption by the silver bromide

present in the film, a latent image is formed. This image corresponds to a topograph of the crystal and is obtained by the developing of the film.

The following films were available: Type NS: no screen, relative speed 700, double coated; Type AX: no screen, relative speed 100, double coated; Type TMX: no screen, relative speed 54, double coated; Type M: no screen, relative speed 30, double coated; Type R: no screen, relative speed 7.5, single coated.

Exposure times were set by trial and error using the fastest film available (NS type). After obtaining a topograph with a suitable level of blackening that allows the best optical contrast around the annealed spots to be observed, the experiment is repeated using a slower (less grainy) type of film (AX type). Since the relative speed ratio of these films is 7:1, the exposure time is seven times as long when AX type is used.

The slower the film the better the resolution, exposures with TMX film were also run. However, proper exposure times were much too long.

Topographs of specimen A and specimen B were thus obtained. They are presented in Plates 1 and 2, respectively. The exposure time of specimen A using AX film corresponds to 45 hours. The topograph of specimen B took a 77 hour exposure time. It was because of these high exposure times that the slower film types (TMX, M, R) were not used in this work. The resolution given by the AX film was acceptable as it showed the structure within some annealed spots. These spots were chosen to be studied.

Interpretation of the Topographs

The strain due to the ion implantation results in a variation of the

Plate 1 Printed topograph of Specimen A. Magnification = 9.

THIS BOOK CONTAINS NUMEROUS PICTURES THAT ARE ATTACHED TO DOCUMENTS CROOKED.

THIS IS AS RECEIVED FROM CUSTOMER.

THIS BOOK CONTAINS SEVERAL DOCUMENTS THAT ARE OF POOR QUALITY DUE TO BEING A PHOTOCOPY OF A PHOTO.

THIS IS AS RECEIVED FROM CUSTOMER.

Plate 1

Plate 2 Topograph of Specimen B. Magnification = 10.

Plate 2

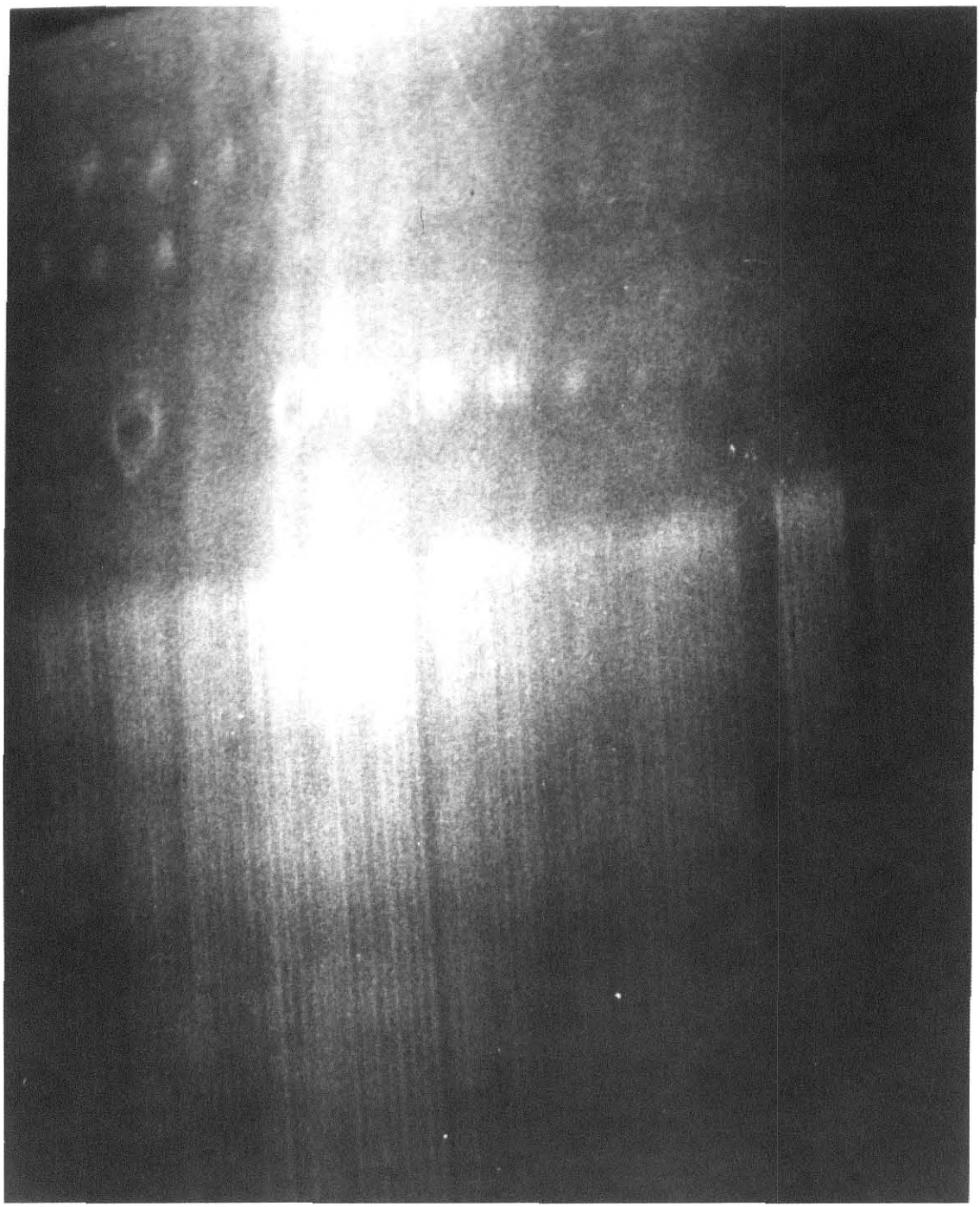

d spacing of the crystal. When laser annealing is performed at a spot, since this is a radial process, the immediate surrounding areas are subject to a rearrangement of the implanted ions and silicon atoms to form planes of symmetry of a smaller d spacing than the one corresponding to the strained crystal. The d spacing of the annealed regions depends on the amount of annealing (energy density used) and the relative size of the implanted ions with respect to the atomic size of the silicon atoms that originally made up the lattice.

Then around an annealed spot there is a transition zone corresponding to the difference of reflectivity by two different d spacings and therefore two different amounts of blackening in the topograph. By finding the angular difference, $\Delta\theta$, of these d spacings in the Bragg reflection law, it is possible to find the variation of the d spacing between the respective zones. This can be taken as a measure of the annealing that has occurred.

Bragg's Law

$$\lambda = 2\, d \sin\theta$$

$$\rightarrow \Delta\lambda = 2 \sin\theta\, \Delta d + 2d \cos\theta\, \Delta\theta$$

yields the relation

$$\frac{\Delta\lambda}{\lambda} = \frac{\Delta d}{d} + \operatorname{cotg}\theta\, \Delta\theta$$

Since monochromatic x-rays were used $\Delta\lambda=0$, and

$$\frac{\Delta d}{d} = -\operatorname{cotg}\theta \cdot \Delta\theta_s,$$

where θ is taken as the Bragg angle, $\theta=34.59746$ degrees of arc in both cases (specimens A and B). $\Delta\theta_s$ corresponds to the variation of the Bragg angle for the damaged region with respect to the Bragg angle of the annealed region. The width of the observed transition zone is proportional to $\Delta\theta_s$. To find the relationship involved, the geometry of the experiment

is used. From Fig. 9:

$$\Delta\theta_s = \frac{W}{R} \sin\theta \text{ (radians)} \quad \begin{matrix}[W]=cm \\ [R]=cm\end{matrix}$$

R is a constant for the geometry, while W measures the width of a line on the film due to the variation of d spacing (d_1 and d_2).

Another variable that has to be considered is the sensitivity of the x-rays, or sensitivity of this method to detect variations of diffracted intensity resulting from the variations of the Bragg angle. The sensitivity is defined as

$$S = \frac{\Delta I}{\Delta\theta}$$

For this purpose, a fixed crystal-film photograph of the diffracted x-ray radiation was taken. A plot of blackening versus position was recorded using a densitometer, Plate 3. Two peaks are observed, they both correspond to Kα radiation diffracted by the crystal, the higher one corresponds to the blackening of the side of the film closer to the crystal, and the other corresponds to the blackening on the opposite side. This effect results from the fact that a double coated film was used.

The blackening level below the second peak was considered to be background noise. Above this noise a Gaussian type of intensity distribution yields a width of 1.00×10^{-2} cm to reach the half maximum; then

$$\Delta\theta = \frac{W \sin\theta}{3.5} = 1.62\times10^{-3} \text{ radians}$$

This is taken as the resolution of the method. The sensitivity is taken as the slope of the curve at this half maximum level,

$$S = \frac{\Delta I}{\Delta\theta_i} = K \frac{\Delta B}{\Delta\theta_i} = 81.4\ K, \quad K\text{: film and development related constant.}$$

A measurement of the angular difference between strained and annealed zones would then render the sought value, $\frac{\Delta d}{d}$. However, this measurement

Figure 9 Variation of the Bragg angle due to variation of d spacing.

FIGURE 9

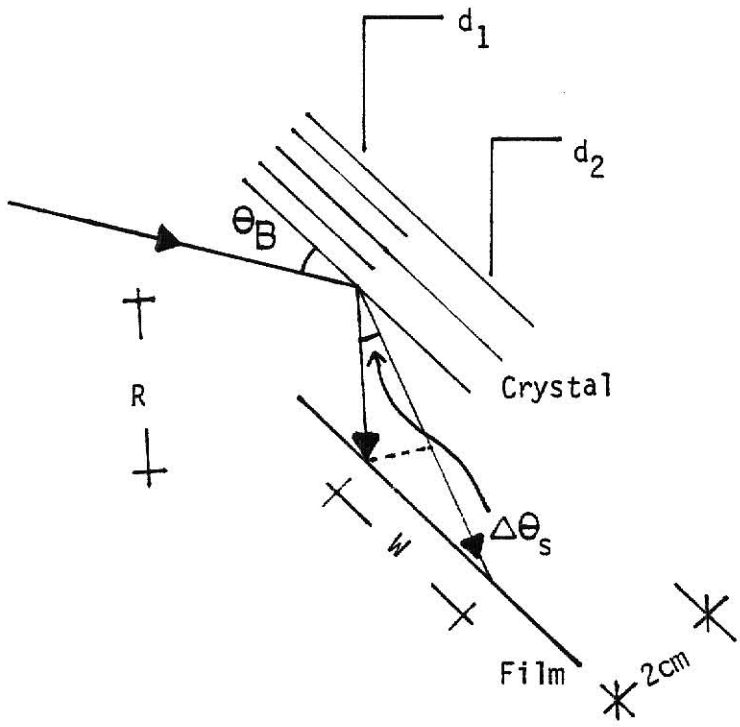

Plate 3 Densitometer graph of diffracted Kα radiation.

Two peaks show up due to double coated film.

PLATE 3

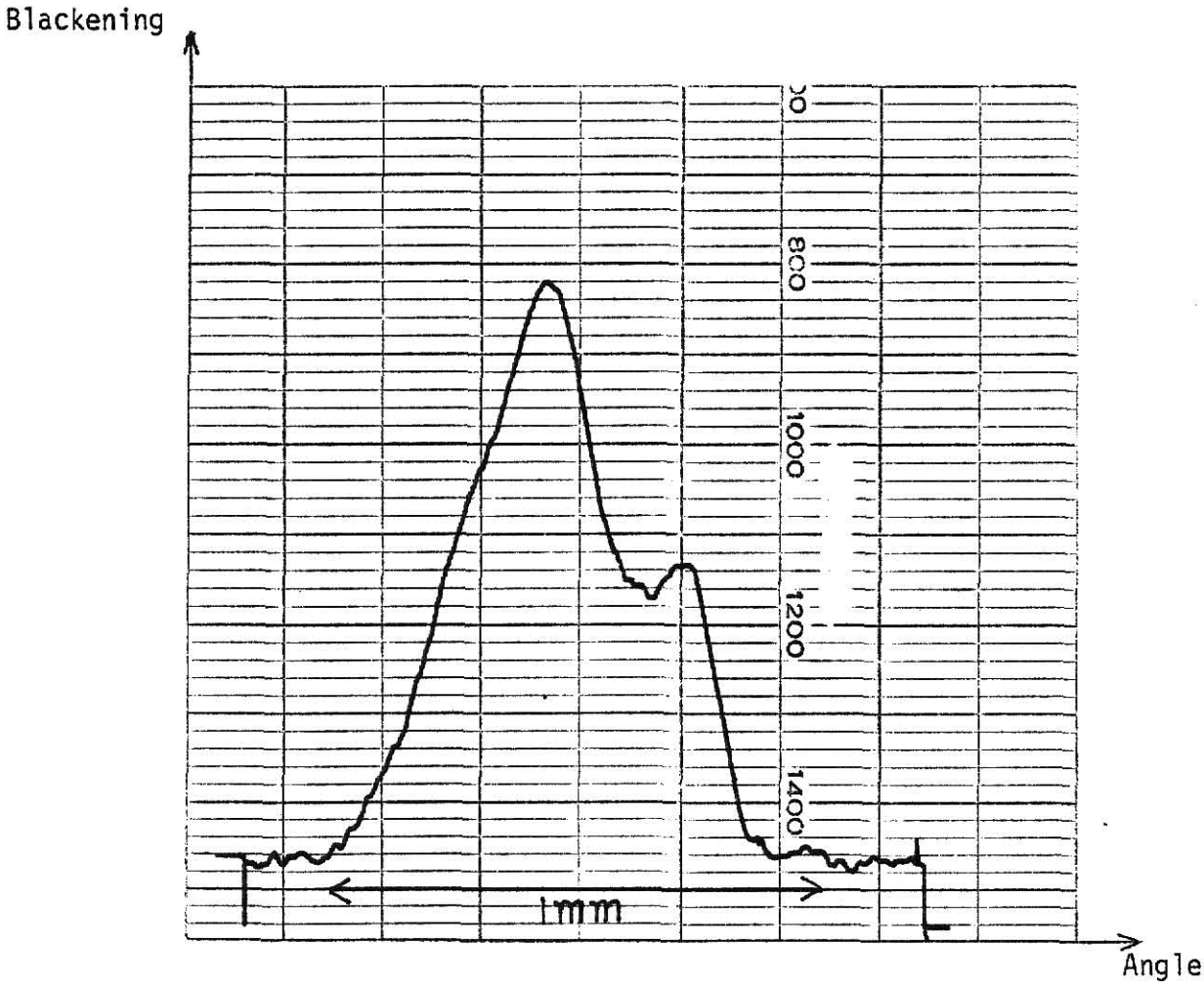

($\Delta\theta_m$) would need to be adjusted considering the sensitivity of the method (S).

Two approaches were devised for this purpose. A densitometer graph (blackening vs. position) could be obtained by scanning horizontally across the annealed spots, using the topographic film. A difference in blackening between the annealed and damaged regions can be calculated (ΔB), and thus

$$\Delta\theta_i = \frac{\Delta B}{81.4}$$

is the angular variation for a given blackening variation limited by the sensitivity of this method. Also, a calibration of position would allow the indirect measurement of $\Delta\theta_m$, by measuring the relative position between the annealed and damaged regions. This corresponds to the width of the transition zone. Then,

$$\Delta\theta_s = \Delta\theta_m - \Delta\theta_i.$$

An alternate method is also viable. Using optical techniques, a measurement of the distance between damaged and annealed regions by observation of contrast could be used as an indirect measurement of the angular difference ($\Delta\theta_m$). Then the strain ($\frac{\Delta d}{d}$) could be calculated as before. However, as discussed in the previous method, it is necessary to know the difference in blackening between the two contrasting zones to calculate the lag ($\Delta\theta_i$) due to sensitivity of this method.

Optical photographs were taken of the annealed spots of specimen A and specimen B. These photographs were taken by a Polaroid system using film Type 57, coupled to an optical microscope. The pictures were all taken using the same magnification, and in addition a photograph of a measuring scale (2mm long with a resolution of 0.01mm) was also taken to be used in the dimensioning of these spots. This allows one to obtain the

actual size of the corresponding spots as seen in the topographs, and to make qualitative observations as to their relative size. Plates 4 and 5 show spots (1,2,3,6,7,8) and (4,5) respectively as labeled in Figure 4 (specimen A). Plates 6 and 7 shows spots 1 and (2,3) respectively as shown in Figure 5 (specimen B).

Plate 4 From bottom up and left to right, optical pictures of spots (1,2,3,6,7,8) of Specimen A. Magnification = 30.

Plate 4

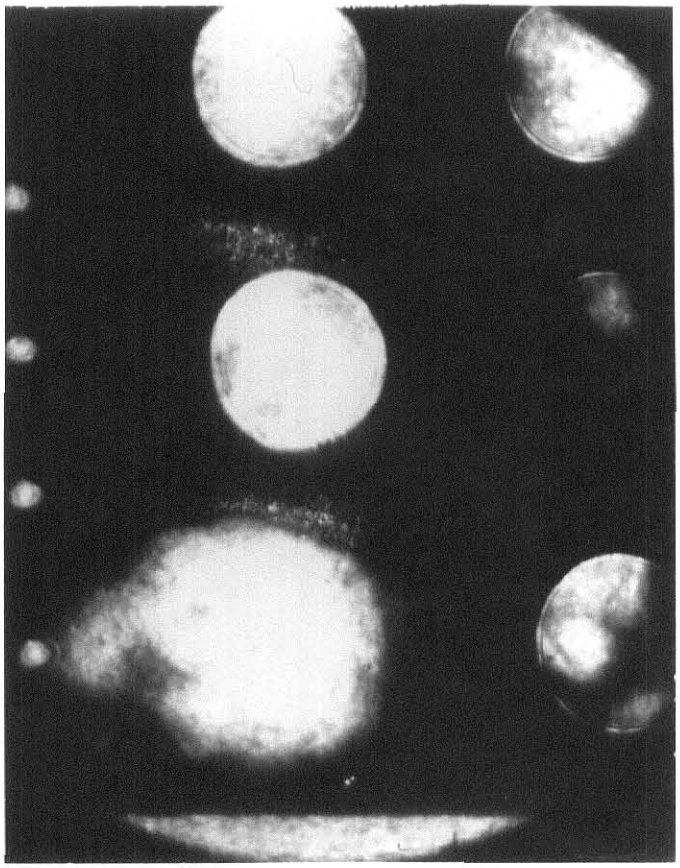

Plate 5 From bottom up, optical pictures of spots 4 and 5 of Specimen A. Magnification = 30.

Plate 5

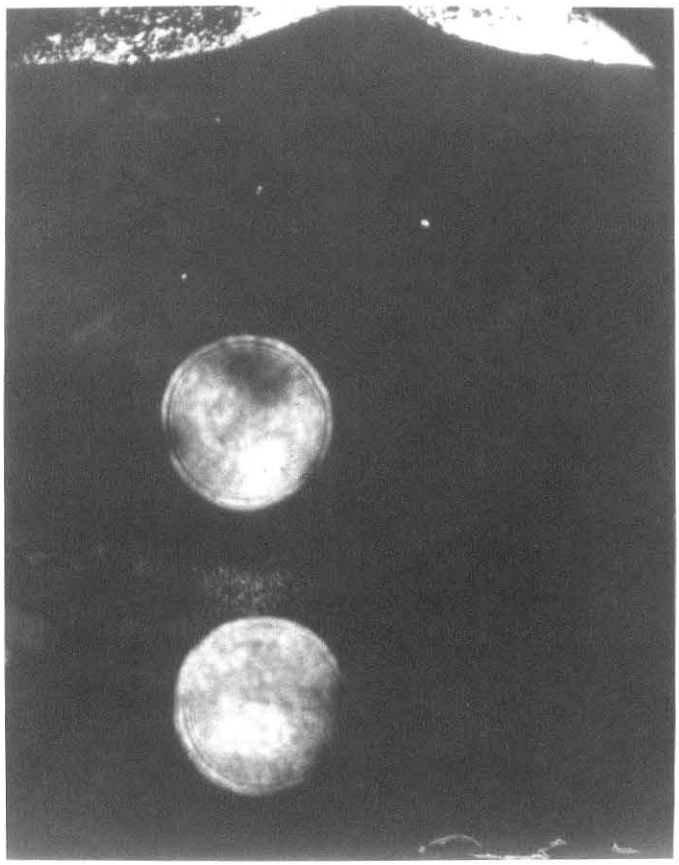

Plate 6 Optical picture of spot A1 of Specimen B.

Magnification = 30.

Plate 6

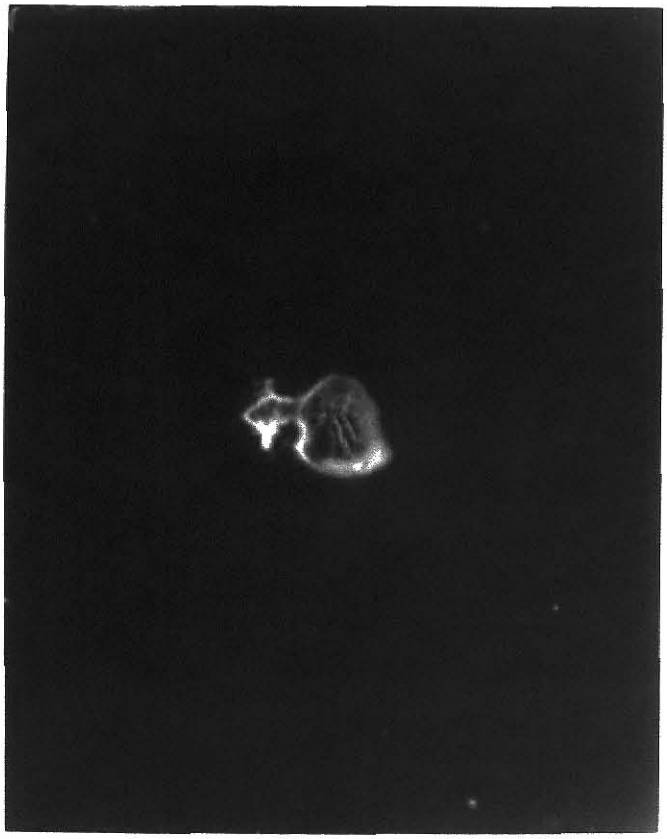

Plate 7 Optical picture of spots 2 and 3 of Specimen B.

Magnification = 30.

Plate 7

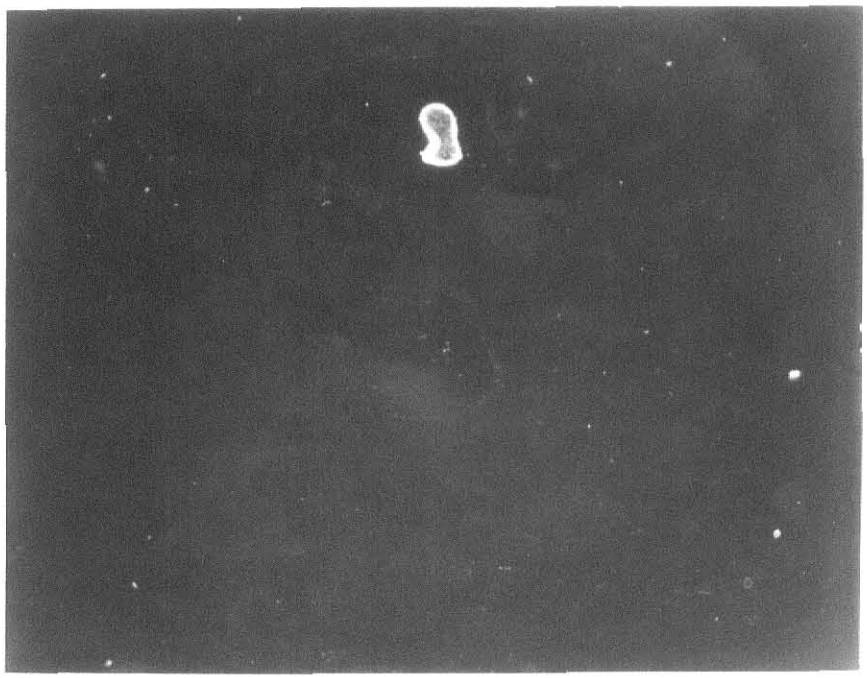

Plate 8 Typical densitometer graph. Three distinctive blackening regions are observed.

PLATE 8

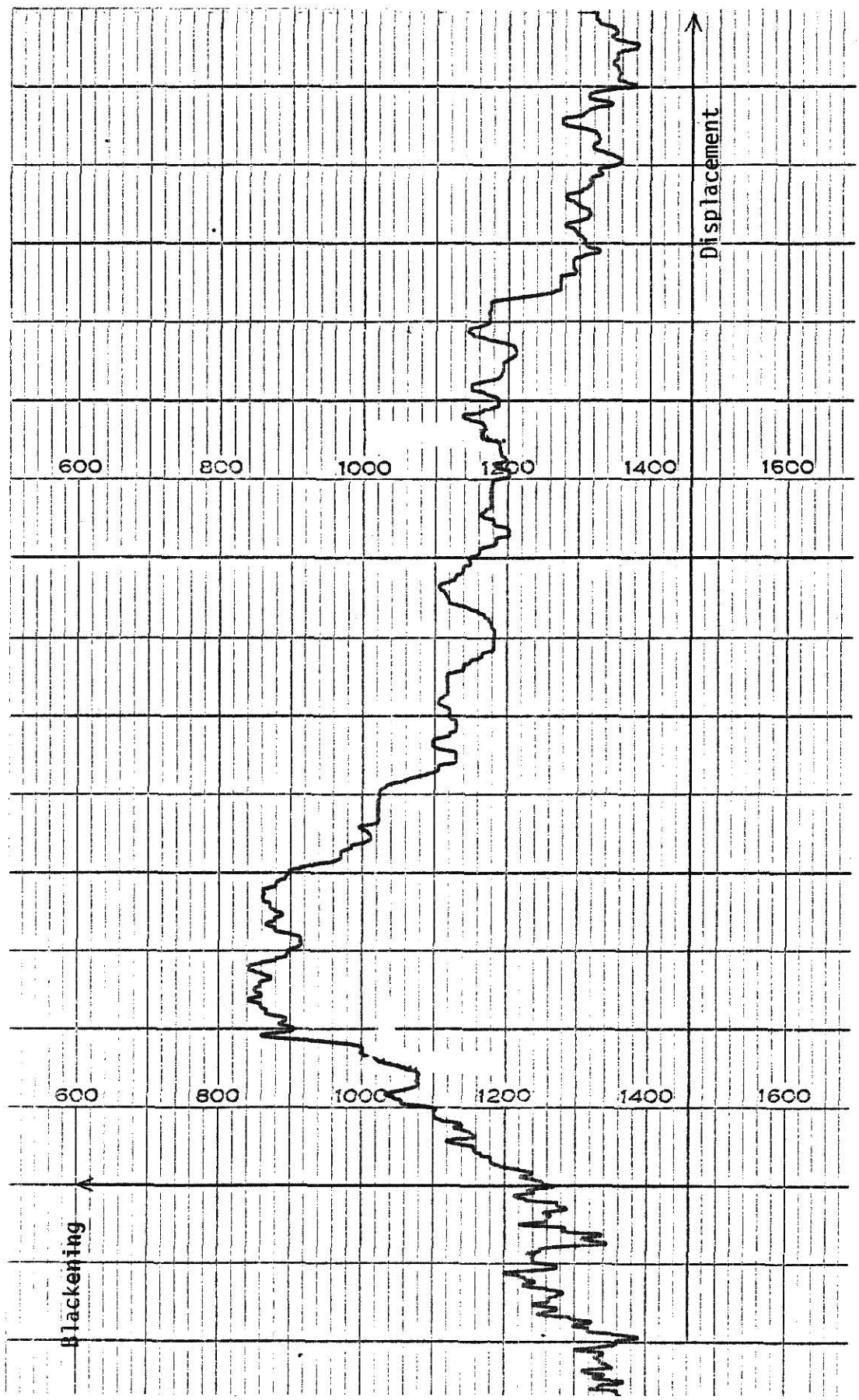
Displacement
600
800
1000
1200
1400
1600
Blackening
600
800
1000
1200
1400
1600

Chapter 3

RESULTS

An analysis of microdensitometer graphs of the annealed spots of the two crystals shows three distinctive zones corresponding to different levels of blackening. The highest reflectance zone is that closest to the spot center, farther from the center is a medium reflectance zone and finally at the greatest distance from the center there is a low reflectance zone. Plate 8 shows a typical microdensitometer graph.

The lowest reflectance zone, that of least blackening, corresponds to the strained crystal. It is fairly uniform in blackening as is the medium zone, with a transition zone between the two. This medium zone is taken as the blackening corresponding to the diffracted intensity from the annealed region.

A measurement of the $\Delta\theta_m$ value was taken from the different microdensitometer graphs corresponding to the transition zone between the annealed and the strained crystal regions and by calculating $\Delta\theta_i$ (through the difference in blackening) a $\Delta\theta_s$ was obtained. This method made it possible to calculate the associated strain, $\frac{\Delta d}{d}$.

The higher reflectance zone was observed to increase its blackening as the laser energy density was increased. This variation was not observed in the annealed region. This high reflectance zone can then be related to the introduction of strain by the excessive energy density used for the anneal. By introducing strain the laser is then producing a zone of imperfection, and as a crystal becomes more imperfect a higher reflectance is observed. J. E. White[10] conducted an experiment in which a quartz crystal was bent to

introduce strain and an increased intensity resulted. A calculation of the strain associated with the transition between the high reflectance and annealed regions was made using the microdensitometer graphs of Specimen B, where higher energy densities were used in the "annealing" process. Results are presented in Table 3 and plotted in Figure 10. This graph is quite similar to the one obtained by White in his experiment and which is presented in Figure 11.

The results obtained for strain, $\frac{\Delta d}{d}$, related for the annealed and un-annealed regions for crystals A and B are presented in Table 4.

Table 3 Introduced strain by laser.

TABLE 3

Introduced Strain by Laser

Spot	$\Delta\theta_s$ rad	$\frac{\Delta d}{d}$	Laser Energy Density (J/cm^2)
A1	17.72×10^{-3}	25.69×10^{-3}	4.6
A2	15.83	22.95	2.3
A3	12.35	17.90	1.7
A5	6.31	9.15	1.2
B2	6.55	9.50	0.9

$(\Delta\theta \pm 1.62 \times 10^{-3})$ radians

$(\frac{\Delta d}{d} \pm 2.35 \times 10^{-3})$

Figure 10 Transition from nearly perfect crystal to a nearly imperfect crystal under excessive laser energy density.

FIGURE 10

Transition from nearly perfect crystal to a nearly imperfect crystal under excessive laser energy density.

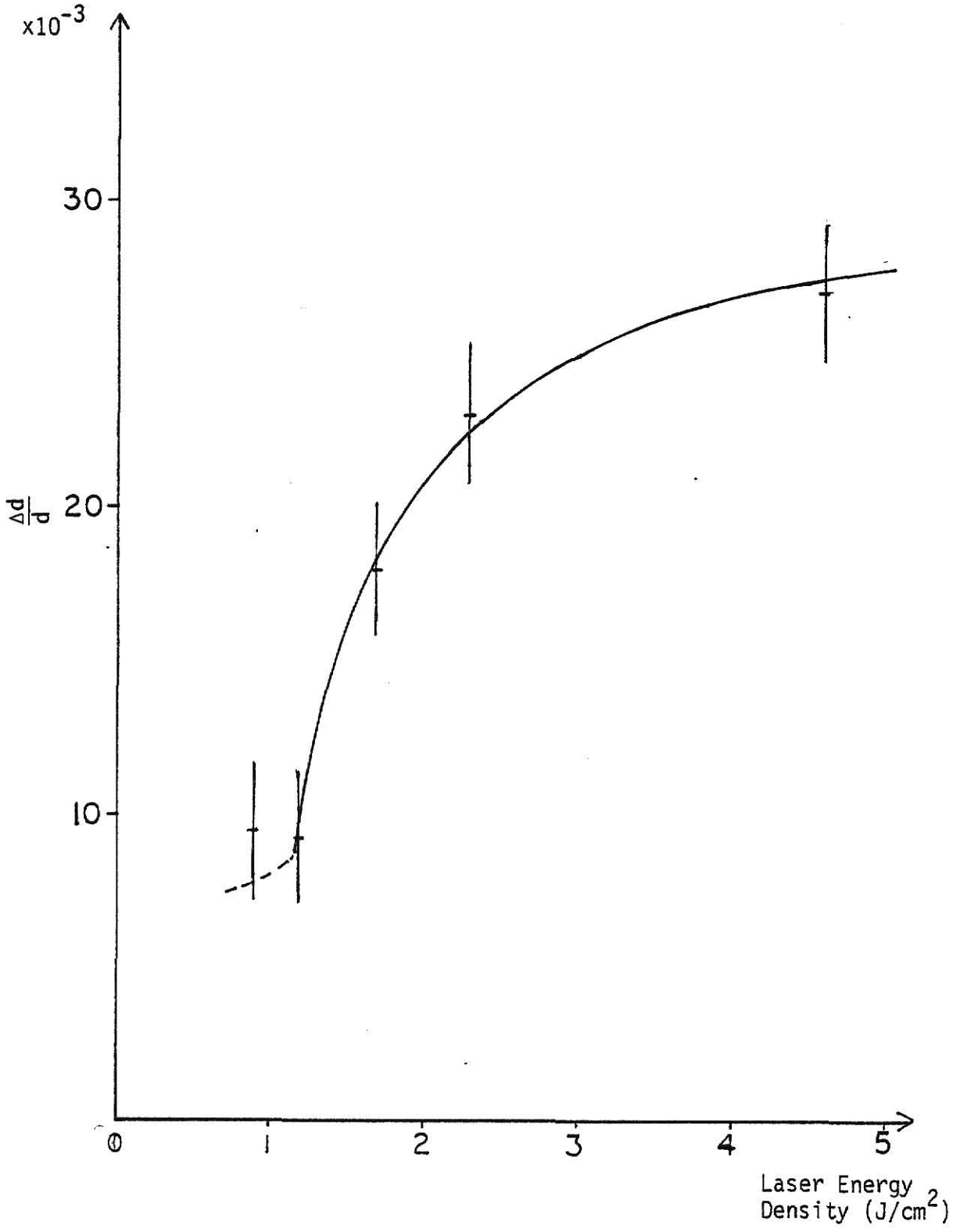

Figure 11 J. E. White experimental result for a transition from a nearly perfect crystal to a nearly imperfect crystal.

FIGURE 11

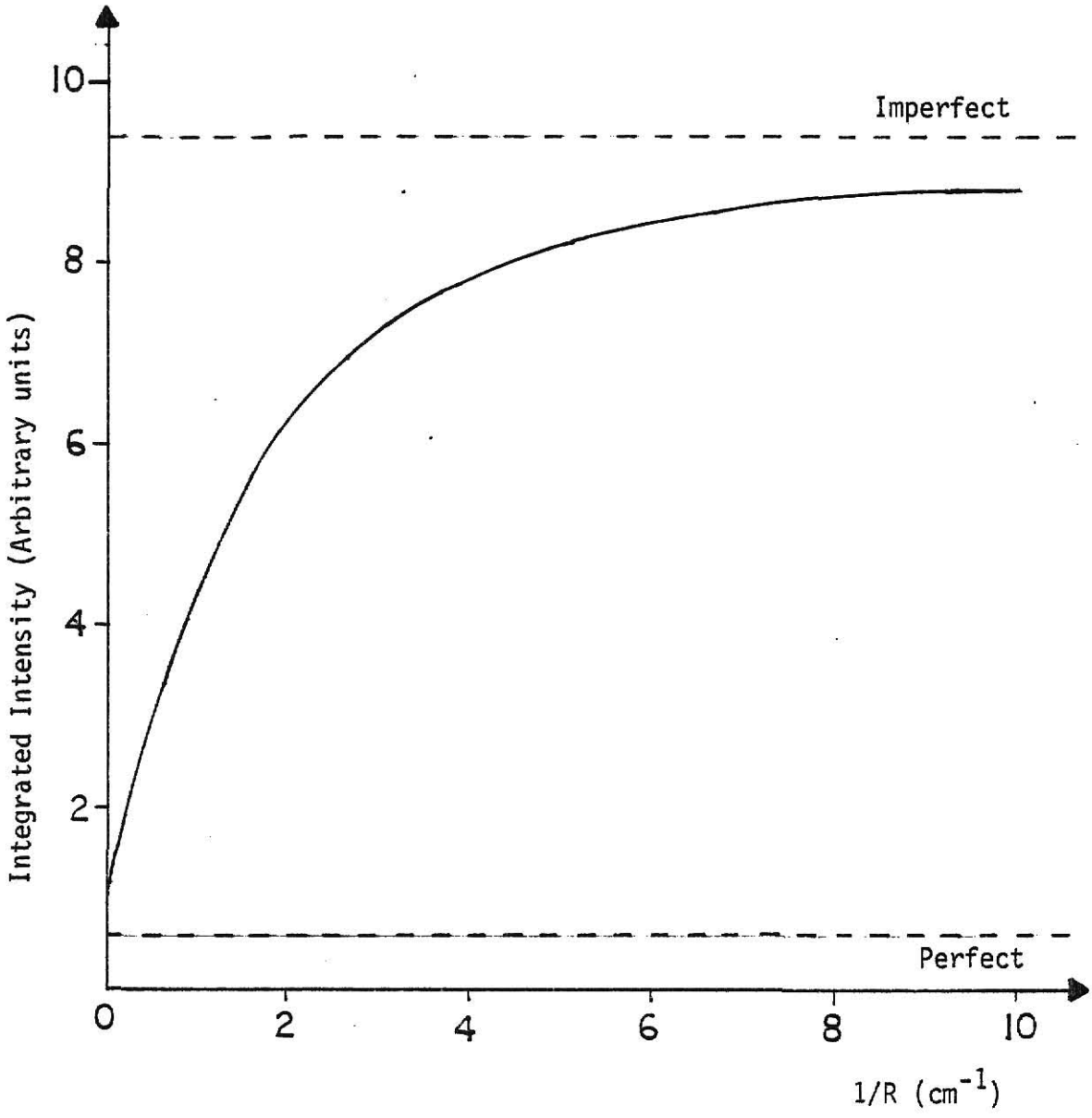
Integrated Intensity (Arbitrary units)
10
8
6
4
2
0
2
4
6
8
10
Imperfect
Perfect
1/R (cm^{-1})

Table 4 Strain associated with annealing.

TABLE 4

Strain Associated With Annealing

Specimen A

Spot	$\Delta\theta_s$ rad	$\frac{\Delta d}{d}$	Laser Energy Density (J/cm^2)
2	3.40×10^{-3}	4.93×10^{-3}	1.15
3	3.01	4.36	0.81
4	3.25	4.71	0.57

Specimen B

Spot	$\Delta\theta_s$ rad	$\frac{\Delta d}{d}$	Laser Energy Density (J/cm^2)
A1	4.17×10^{-3}	6.04×10^{-3}	4.6
A4	3.31	4.79	1.2 (2 shots, 1.2 each)
A5	3.04	4.40	1.2
A6	3.25	4.71	0.69
A7	3.86	5.59	0.22 (2 shots, 0.22 each)
B2	4.24	6.15	0.9

$(\Delta\theta \pm 1.62 \times 10^{-3})$ radians

$(\frac{\Delta d}{d} \pm 2.35 \times 10^{-3})$

Chapter 4

OBSERVATIONS AND CONCLUSIONS

Specimen A

Plate 1 shows the printed topograph of Specimen A. Spots 1,6 and 7 as labeled in Figure 5 do not appear on the topograph. The rest of the spots show annealing since they are observed in the topograph. Some contrast bands are observed between spots in the optical micrograph as well as in the topograph.

Spots 2,3 and 4 of Specimen A show a similar contrast with respect to the strained, surrounding region, but spots 5 and 8 exhibit a rather low contrast. This can be related to the lower energy density value of the annealing (0.39 J/cm^2 and 0.21 J/cm^2, respectively).

A dimensional comparison between the various spots as observed in the optical micrographs and the topograph show that the size and shape are maintained. The magnification of the topographic pictures was established to be 10.

Specimen B

The printed topograph of Specimen B, Plate 2, shows that only the spots B12, B13 and C18 do not show contrast. On spots A1 and A2 sputtering of the crystal by the high laser energy density is observed in the optical micrograph, as well as in the topograph.

In most cases the contrast is observed to be good. The zone that was annealed in successive spots, one half of their radii apart, is observed with good contrast. The existence of this large annealed area facilitated

the orientation of this crystal during the experimental set-up, since a higher intensity was diffracted than in Specimen A.

The horizontal divergence of the slit, 7 minutes of arc equal to $2x10^{-3}$ radians, proved to be a rather small factor not affecting the resolution.

The sensitivity, $\frac{\Delta I}{\Delta \theta}$, was quite adequate since the $\Delta\theta_i$ associated with the variation of contrast was consistently of the order of 10^{-4} radians, while the $\Delta\theta_s$ values were of the order of 10^{-3} radians.

The vertical divergence, 3.77 degrees of arc, produced a broadening of horizontal lines. To avoid introducing significant errors due to this divergence the microdensitometer runs on the spots were done horizontally across the annealed spots.

The fact that the film was placed parallel to the crystal has the advantage of yielding an undistorted topograph of the crystal. A disadvantage of this set-up, however, arises from the fact that the film used (AX type) is double coated and since the diffracted beam reaches the film at an angle (θ_B a second, undesirable, image is recorded on the side of the film furtherest from the crystal. The x-ray absorption by the emulsion on the closer side to the crystal and the celluloid helps to alleviate the problem by diminishing the intensity. This second image is shifted 0.26mm to the right side of the spots. However, since the diameter of these spots is about 1mm, the shifting is not a major factor in measuring strain. The measurements of $\Delta\theta_m$ would not be greatly affected if done to the left of the spots. In fact measurements done on the right side, where this shift is observed yielded the same results within the resolution of the method.

This problem could be avoided using single coated films. However, in our experiment, this was not practical because single coated films are much

slower and the exposure times would be too high. An alternate way to deal with the problem would be to place the film perpendicular to the diffracted beam, at an angle ($90-\theta_B$) with respect to the crystal. This would render distorted topographs, but since a smaller area of the film would be blackened a faster exposure time would result. On the other hand, a slower film would have the additional advantage of having a lower noise blackening level.

These considerations, then, should be taken into account in any future work using this method. With a better resolution and considering more spots with laser energy densities ranging from 0.5 J/cm^2 to 1.4 J/cm^2 perhaps an optimal value could be found for the energy density to anneal the strained crystal. Larger area spots would also facilitate the use of the microdensitometer.

Chapter 5

SUMMARY

An experimental method was devised to obtain x-rays topographs in the Bragg reflection geometry of two single silicon (400) crystals that had been ion implanted and laser annealed on various spots using different energy densities. In addition to the topographs, microphotographs were taken using a microscope coupled to a Polaroid camera. A calibration scale was also photographed, using the same magnification, to make dimensional measurements of the optical images of the spots.

Copper Kα radiation was used as source. This radiation was collimated and reached the crystal at the corresponding Bragg angle and the diffracted beam was absorbed by x-ray film (AX type) placed parallel to the diffracting planes. Crystal and film were coupled in a horizontal back and forth displacement that produced a scanning of the crystal by the x-rays, thus producing a topograph.

The crystal was oriented to obtain a maximum diffracted intensity varying the angle of incidence of the radiation. Once a maximum intensity was recorded, by a Geiger counter, the angle was very slowly decreased until a half intensity count is registered by the Geiger counter. This enhances the sensitivity of the x-rays to detect the variations of the interplanar spacing (d) associated with the strain introduced by the ion implantation and its variation due to the annealing done by the laser. This variation in turn produces a variation $\Delta\theta$ of the Bragg angle. From Bragg's Law

$$\frac{\Delta d}{d} = -\text{cotan } \theta_B \, \Delta\theta$$

The variation $\Delta\theta$ leads to a variation of diffracted intensity from annealed and unannealed regions, resulting in a variation of film blackening. A transition zone is then observed between annealed and unannealed zones corresponding to a $\Delta\theta$ value.

Microdensitometer runs of the spots recorded on the topographs made it possible to calculate $\Delta\theta$ with a systematic error of 1.62×10^{-3} radians and using the relation given above a strain value, $\frac{\Delta d}{d}$, was obtained for different spots on both crystals.

In one crystal, where higher energy densities were used, it was observed that the excessive energy density not only produced a zone of annealing, but also another zone immediately around the center of the spot where strain was introduced by the crystal. This zone shows a higher reflectance than the annealed and unannealed zones, such higher reflectance was associated with the transition from a nearly perfect (annealed) crystal to a nearly imperfect (strained) crystal. It was noted by J. E. White[10] in an experiment where he introduced strain in a nearly perfect crystal by bending it that an increase in reflectance of x-rays occurs as the crystal becomes nearly imperfect. The transition from a nearly perfect crystal to a nearly imperfect crystal by introducing strain using a laser beam was then observed in this experiment.

The method yielded values of strain with a systematic error of 2.35×10^{-3}.

BIBLIOGRAPHY

1. Carter, G. and Grant, W. A., Ion Implantation in Semiconductors (John Wiley and Sons, New York, 1976) p. 187.

2. Johnson, W. S. and Gibbons, J., Projected Range Statistics in Semiconductors, Stanford University Bookstore, 1969.

3. Lindhard, J., Scharff, M. and Schiott, H. E., Matt. Fys. Medd. Danske Videnskab, 33 (1963), No. 14.

4. Lee, M. C., Lo, H. W., Aydinli, A. and Compaan, A., Department of Physics, Kansas State University, App. Phys. Lett. 38(7), 1 April 1981.

5. Lo, H. W. and Compaan, A., Raman Measurements of Lattice Temp. During Pulsed Laser Heating of Silicon, Phys. Rev. Lett. V.44, No. 24, June 16, 1980.

6. Cullity, B. D., Elements of X-Ray Diffraction, 2nd Edition, pp. 501, 276.

7. Aydinli, A., Lo, H. W., Lee, M. C. and Compaan, A., Phys. Rev. Lett., Vol. 46, No. 25, June 22, 1981.

8. Wyckoff, R. W., Crystal Structures, 2nd Edition, Vol. 1, page 26, Inter-Science Publishers, 1963.

9. Straumanis, M. E., AKA, E. Z. Structure Reports, Vol. XIII, p. 156, 1950.

10. White, J. E., J. Appl. Phys. 21, 855 (1950).

X-RAY TOPOGRAPHY OF LASER ANNEALED ION IMPLANTED SILICON CRYSTALS

by

ARGENIS PRIETO

Lic. en Fisica - Unversidad de Oriente, 1979
Cumana, Venezuela

AN ABSTRACT OF A MASTER'S THESIS

submitted in partial fulfillment of the

requirements for the degree

MASTER OF SCIENCE

Department of Physics

KANSAS STATE UNIVERSITY

Manhattan, Kansas

1983

ABSTRACT

Two single silicon crystals (100) ion implanted, one with Si^+ ions and the other with As^+ ions were laser annealed using different energy densities.

A Bragg reflection geometry method was used to obtain topographs of both crystals. A study of these spots on the topographs using a microdensitometer made it possible to calculate the strain associated with the annealed and unannealed regions with a systematic error of 2.35×10^{-3}.

For laser energy densities higher than 0.9 J/cm^2 strain was introduced by the laser producing a higher reflectance zone. The transition from a nearly perfect crystal to a nearly imperfect crystal due to strain introduced by the laser beam was observed.

X-ray topographs of spots gave similar appearance to that seen from optical pictures.